Dalton Transactions

Mechanochromism in the luminescence of novel cyclometalated platinum(II) complexes with α-aminocarboxylates

Journal:	*Dalton Transactions*
Manuscript ID	DT-ART-11-2015-004516.R1
Article Type:	Paper
Date Submitted by the Author:	22-Jan-2016

Complete List of Authors:	Ohno, Keiji; Saitama University, a. Department of Chemistry, Graduate School of Science and Engineering Yamaguchi, Shohei; Saitama University, a. Department of Chemistry, Graduate School of Science and Engineering Nagasawa, Akira; Saitama University, a. Department of Chemistry, Graduate School of Science and Engineering Fujihara, Takashi; Saitama University, Comprehensive Analysis Center for Science

Journal Name

ARTICLE

Mechanochromism in the luminescence of novel cyclometalated platinum(II) complexes with α-aminocarboxylates

Received 00th January 20xx,
Accepted 00th January 20xx

DOI: 10.1039/x0xx00000x

www.rsc.org/

Keiji Ohno,[a] Shohei Yamaguchi,[a] Akira Nagasawa,[a] and Takashi Fujihara [b]*

Six novel phosphorescent cyclometalated platinum(II) complexes with α-aminocarboxylato, [Pt^{II}(ppy)L] (ppy = 2-phenylpyridinato, LH = Gly, Ala, Leu, Ile, Phe, Sar), were synthesized, and the structures were determined by the X-ray crystallography. [Pt^{II}(ppy)L] (LH = Gly, Ala) in crystals are in monomeric structures and stack through π–π interactions to form columns, and the features of the luminescence are similar to each other and those in solution, suggesting little influence of the π–π interactions on the luminescence. [Pt^{II}(ppy)Leu] has a dimeric structure through Pt–Pt interaction. [Pt^{II}(ppy)Sar] showed two pseudo-polymorphs, one of which contains both monomeric and dimeric forms, while the other consists of only dimeric units. Intra-dimer π–π interactions were observed in both the dimeric units. [Pt^{II}(ppy)L] (LH = Leu, Ile, Phe) in the solid state displayed different spectral patterns of luminescence from those in solution, suggesting that the dimeric structures through Pt–Pt interaction in the solid state are dissociated into the corresponding monomeric ones in solution. The complexes expect [Pt^{II}(ppy)Phe] in the solid state exhibited reversible luminescent mechanochromism in response to the mechanical grinding and treatment with a few drops of solvent. These phenomena are derived from the change in the energy level of the triplet state due to the change in the extent of intermolecular interactions appeared as the crystalline–amorphous phase conversion.

Introduction

Phosphorescent cyclometalated transition-metal complexes have attracted much attention because of their potential applications, including organic light-emitting diodes (OLEDs), oxygen sensors, and biological cell imaging.[1] These complexes exhibited strong luminescence and remarkable changes in emission colour depending on electronic properties of substituents on the cyclometalating ligand.[2] Some of these Pt^{II} complexes, which have filled 5d_z^2 orbitals perpendicular to the coordination plane, were assembled through intermolecular Pt–Pt and/or π–π interactions in the solid state, and interestingly these interactions led to characteristic luminescence different from that in solution.[3] Particularly, Pt–Pt interaction depends on the Pt···Pt distance, and structural transformation to different magnitude of Pt–Pt interaction triggers changes in the emission colour.[4] Actually, complexes in polymorphisms showed distinct absorption and emission colours by changing over the molecular arrangements.[5]

Many investigations on chromic behaviour have been reported.[6] Above all, luminescent chromic phenomena in response to external stimuli, such as mechanical forces (mechanochromism),[6a,6b,6f] heat (thermochromism),[6c,6f] and sorption of volatile organic solvents (vapochromism)[6b,6d,6e] are among hot topics. These intriguing stimuli-responsive luminescent chromisms are expected to be important factors for applications such as sensing and recording. These external stimuli-triggered changes in luminescence are mainly induced by transformations in the crystal structures,[6a,7] and thus intermolecular interactions play significant roles in these luminescent chromic behaviours.

In the present study, we describe the syntheses, structures, stimuli-responsive luminescent chromisms, and changes in emission colours induced by pseudo-polymorphs of six novel cyclometalated Pt^{II} complexes with α-aminocarboxylato, [Pt^{II}(ppy)L] (ppy = 2-phenylpyridinato, LH = Gly (**1**); Ala (**2**); Leu (**3**); Ile (**4**); Phe (**5**); Sar (**6**)) (Scheme 1).

[a] *Department of Chemistry, Graduate School of Science and Engineering, Saitama University, 255 Shimo-Okubo, Sakura-ku, Saitama 338-8570, Japan.*
[b] *Comprehensive Analysis Center for Science, Saitama University, 255 Shimo-Okubo, Sakura-ku, Saitama 338-8570, Japan.*

† Footnotes relating to the title and/or authors should appear here.
Electronic Supplementary Information (ESI) available: [details of any supplementary information available should be included here]. See DOI: 10.1039/x0xx00000x

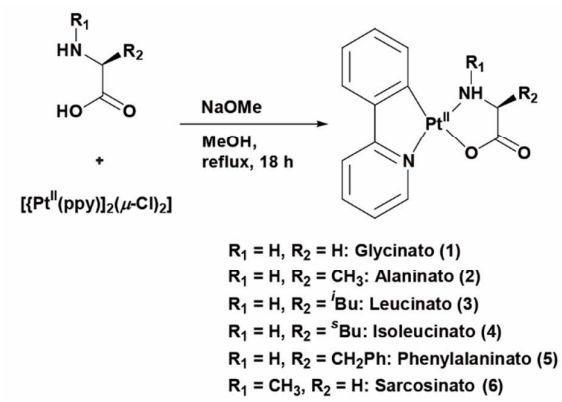

Scheme 1. Six cyclometalated Pt^{II} complexes with α-aminocarboxylato (L), $[Pt^{II}(ppy)L]$.

Results and Discussion

Syntheses and Characterisation in solution

The complexes **1–6** were prepared in high yields by the reaction of the precursor Pt^{II} dichlorido-bridged dimer, $[\{Pt^{II}(ppy)\}_2(\mu\text{-}Cl)_2]$, with corresponding α-aminocarboxylic acid in the presence of NaOMe (Scheme 1).

The ^{1}H NMR spectra in DMSO-d_6 suggested that the existence of a 1:1:1 complex of Pt^{II} and aminocarboxylate (L^-) and ppy^-, from the integral intensities of the signals and absence of O*H* of L and *o*-phenyl proton of ppy.

In solution, little electronic effect of the substituents R_1 and R_2 on the photophysical properties are revealed by UV-Vis absorption spectra in DMSO (Fig. 1A), and emission spectra (λ_{ex} = 400 nm) in DMSO and MeOH/EtOH mixed solution (v/v = 1:1) at room temperature (Fig. 1B and S1 ESI†, respectively, Table 1), and emission spectra (λ_{ex} = 400 nm) in a rigid solvent glass of a MeOH/EtOH mixed solution (v/v = 1:1) at 77 K (Fig. 1C, Table 1). No emission spectrum of **1** at 77K was obtained due to no solubility in solutions expect DMSO. Complexes showed a very similar pattern and positions (maximum wavelength) to each other in each of UV-Vis absorption and emission spectra. Characteristic absorption bands in the range of 300–400 nm are assigned to a mixed transition of ^{1}MLCT and π–π* inside the ppy^- moiety as supported by TD-DFT study (see below). The luminescence in DMSO and MeOH/EtOH mixed solution at r.t. showed vibronic-structured emission centred at ca. 510 and 505 nm, respectively, suggesting little effect of solvent on luminescence. The emission bands are attributed to a mixed transition of ^{3}MLCT and ^{3}LC.[2,3a] The emission spectra at 77 K exhibited well-resolved vibronic-structured emission profiles. The vibronic intervals are ca. 1200 and 1400 cm^{-1} at r.t. and 77 K, respectively. Quantum yields of **1–6** in DMSO at r.t. (λ_{ex} = 400 nm) are similar to each other (Φ_{PL} = 0.01), while **2–6** in MeOH/EtOH glass at 77 K (λ_{ex} = 400 nm) showed high yields in the range of 0.73–0.79 (Table 1). These results indicate no electronic effect of R on luminescent properties. The emission spectral pattern and quantum yields are comparable to those of other reported cyclometalated complexes.[3c]

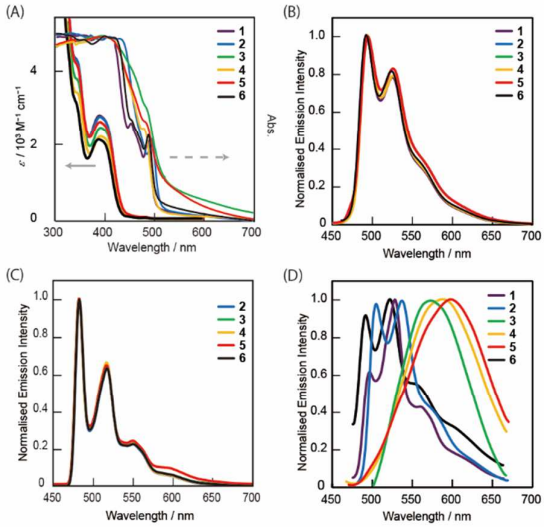

Fig. 1 UV-Vis absorption spectra in DMSO (1.0×10^{-5} M) and in the solid state (pristine samples) at room temperature(A), normalised emission spectra (λ_{ex} = 400 nm) in DMSO (1.0×10^{-5} M) at room temperature (B) and in MeOH and EtOH mixed solution (1.0×10^{-5} M) at 77K (C), and normalised emission spectra of crystals (λ_{ex} = 450 nm) (D) of **1** (purple), **2** (blue), **3** (green), **4** (yellow), **5** (red), and **6** (black).

Pristine samples in the solid state (for the preparations, see below) showed red-sifted bands at 400–600 nm in UV-Vis absorption spectra, compared to those in solution. Emission spectra of **1**, **2**, and **6** displayed similar pattern to ones in solution with two intense and sharp bands in the rage of 450–550 nm (Figs. 1B and 1D, Table 2), suggesting that the luminescence in the solid state originates from monomeric form. Luminescence of **3–5** showed broad bands centered at ca. 600 nm with different patterns from those in solution (Figs. 1B and 1D, Table 2), and the difference is derived from intermolecular Pt···Pt interaction in crystals (see below).

Table 1. Absorption maxima (nm) of **1–6** in DMSO at room temperature, and emission maxima (nm) and quantum yield (Φ_{PL}) of **1–6** in DMSO at room temperature, in MeOH/EtOH mixed solution at r.t and at 77 K.

Complex	Temp.	In DMSO[a]			In MeOH/EtOH[a]	
		λ_{abs} [nm] (ε/$M^{-1}cm^{-1}$)	λ_{em} [nm][b]	Φ_{PL}[b]	λ_{em} [nm][b]	Φ_{PL}[b]
1	r.t.	316 (sh, 8500), 344 (sh, 4300), 380 (2800)	493, 525, 560(sh)	0.01	–[b]	
2	r.t.	318 (sh, 7900), 347 (sh, 4200), 391 (2800)	494, 526, 560(sh)	0.01	489, 521, 560(sh)	0.07
	77K				483, 518, 550, 600(sh)	0.78
3	r.t.	317 (sh, 6500), 345 (sh, 3400), 392 (2200)	494, 526, 560(sh)	0.01	489, 521, 560(sh)	0.02
	77K				482, 517, 549, 599(sh)	0.79
4	r.t.	316 (sh, 8100), 345 (sh, 4200), 391 (2600)	494, 526, 560(sh)	0.01	489, 521, 562(sh)	0.01
	77K				483, 517,550, 599(sh)	0.77
5	r.t.	316 (sh, 6500), 344 (sh, 3400), 391 (2200)	494, 525, 560(sh)	0.01	488, 520, 561(sh)	0.07
	77K				483, 517, 550, 599(sh)	0.73
6	r.t.	318 (sh, 6000), 341 (sh, 3200), 388 (2100)	492, 524, 560(sh)	0.01	489, 520, 564(sh)	0.06
	77K				483, 517, 550, 600(sh)	0.77

[a] 1.0×10^{-5} M; [b] λ_{ex} = 400 nm; [c] Not measured due to less solubility in solvent expect DMSO.

The time-dependent density functional theory (TD-DFT) calculation using the optimised geometrical parameters of the ground state of **1** in DMSO were performed. The dominant frontier molecular orbitals (MOs) are shown in Fig. 2. The energy levels and their relative compositions are shown in Fig. 3 and Table S1 ESI†, and the calculated electronic transitions and their energies together with the experimental absorption maxima are summarised in Table 3. The lowest unoccupied molecular orbital (LUMO) and LUMO+1 are lying mainly on ppy^- moiety and slightly on Pt^{II} centre. The highest occupied molecular orbital (HOMO), HOMO−2, and HOMO−4 consist significantly of $d\pi$(Pt) and $\pi(ppy^-)$ orbitals with some extent of contributions of π and σ orbitals on COO^- moiety of glycinato ligand. On the other hand, electrons of HOMO−1 localise on d_z^2 orbital of Pt^{II} centre. The calculated spectral pattern accord with the experimentally obtained spectrum (Fig. S2, ESI†), and the absorptions in the range of 300-400 nm are attributed to excitations HOMO→LUMO, HOMO−1→LUMO, HOMO→LUMO+1, and HOMO−4→LUMO, suggesting mixed transitions of ^{1}MLCT and π–π* inside the ppy^- moiety. These results indicate little electronic effect of R_1 and R_2 on the spectroscopic properties even in solution, where strong intermolecular interactions with other complexes seen in the solid state are negligible.

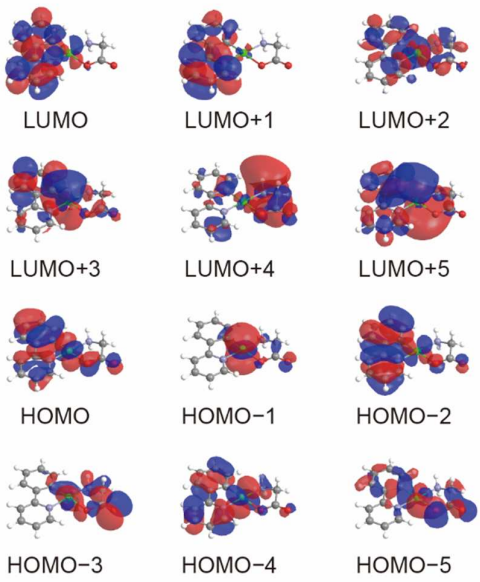

Fig. 2 Selected frontier molecular orbitals (MOs) of the optimised **1** in DMSO.

Table 2. Emission maxima (nm), quantum yield (Φ_{PL}), and lifetime τ_{em} (τ_{em}, μs) of **1**–**6** in the solid state.

Complex	Crystal	Pristine			Ground			Treated
	λ_{em} [nm][a]	λ_{em} [nm][a]	Φ_{PL}[a]	τ_{em} [μs][b]	λ_{em} [nm][a]	Φ_{PL}[a]	τ_{em} [μs][b]	λ_{em} [nm][a]
1	528	496, 528	0.14	0.81	616	0.18	0.73	496, 528
2	537	504, 536	0.02	0.76	605	0.03	0.67	503, 536
3	569	574	0.09	0.60	597	0.04	0.55	574
4	572	587	0.22	1.38	592	0.03	1.07	575
5	591	597	0.09	0.82	597	0.05	1.07	597
6	491, 522[c], 533[d]	492, 522	0.05	0.64	498, 526, 578	0.02	0.76	490, 522

[a] λ_{ex} = 450 nm; [b] λ_{ex} = 450 nm; [c] Crystal-G; [d] Crystal-Y.

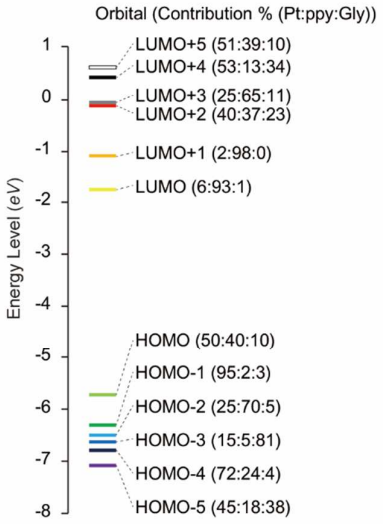

Fig. 3 The energy levels of orbitals and their relative compositions of the optimised **1** in DMSO.

Table 3. Experimental and calculated absorption maxima (nm), transition energy (eV), oscillator strength (f_{calcd}), and major contribution of **1**.

λ_{ex} / nm	λ_{calcd} / nm	E / ev	f_{calcd}	major contribution
390	388	3.20	0.039	HOMO → LUMO (97%)
344	340	3.65	0.007	HOMO–1 → LUMO (98%)
316	314	3.95	0.012	HOMO → LUMO+1 (48%) HOMO–4 → LUMO (17%)

Structures and the luminescent mechanochromism of [Pt^{II}(ppy)Gly] (1) and [Pt^{II}(ppy)Ala] (2) in the solid state

The pristine samples of **1** and **2** were obtained by addition of hexane into solutions of the corresponding complexes. Solvent vapour diffusion provided yellow-green crystals suitable for X-ray crystallographic analyses: Et_2O into the DMSO solution for **1**, and toluene into the THF-MeOH mixed solution for **2**. The data are summarised in Table S2, ESI†.

The crystal structures of **1** and **2** are shown in Fig. 4. There were monomeric neutral complexes with no intermolecular Pt–Pt interactions, and the Pt^{II} centres adopted a square-planar coordination geometry composed of $C_1N_2O_1$ in *trans*-(*N*,*N*)-configuration.

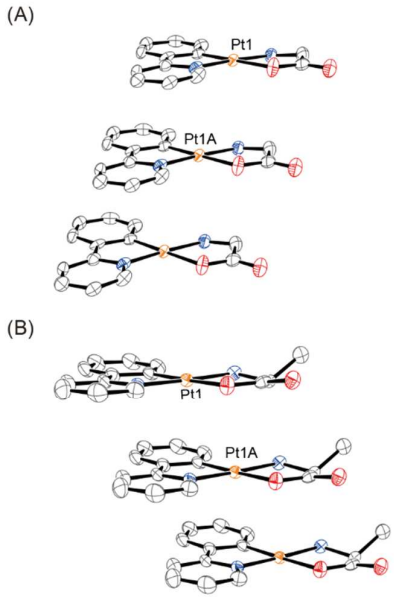

Fig. 4 Stacked structures of monomers of **1** (A) and **2** (B) in 1D-columns with thermal ellipsoids at the 50% probability level. Hydrogen atoms are omitted for clarity.

The complexes were assembled into a one-dimensional (1D) columnar fashion along *b* and *a* axes for **1** and **2**, respectively, with a face-to-face arrangement through intermolecular π–π stacking interactions. The interplanar distances between two ppy planes were 3.44 Å and 3.54 Å for **1** and **2**, respectively. No Pt–Pt interactions are considerable, because the intermolecular Pt···Pt distances (4.19 Å and 4.09 Å for **1** and **2**, respectively) were longer than twice the van der Waals radius of Pt (3.50 Å).

The powder X-ray diffraction (XRD) analyses of the crystal and pristine samples of **1** reveal that the pristine sample have crystalline state with a similar molecular arrangement to one in crystals. Both these samples showed similar typical lamella reflections of a multilayered structure to each other,[8] and the reflection pattern coincides with the simulated pattern

obtained from the X-ray crystallography. Both samples exhibited reversible crystalline–amorphous phase conversion by mechanical grinding and by treatment with solvent, for forward and backward changes, respectively (Fig. 5A). When a sample was ground (details of procedure: see Experimental section), the signals of the ground sample exhibited weak and broad reflections corresponding to the patterns for amorphous phase. Treating the ground sample with solvent (hereafter solvent-treated sample) restored the reflections to the original patterns. These changes are not caused by adsorption and desorption of solvate molecules, because no lattice solvent molecule was found in the crystal samples by the results of thermogravimetric analyses (TGA) (Fig. S4, ESI†).

The pristine sample of **2** showed similar molecular arrangement to that of its crystal sample, and both samples exhibited reversible crystalline–amorphous phase conversion by grinding and treatment with solvent, similar to that of **1** (Fig. S3 ESI†).

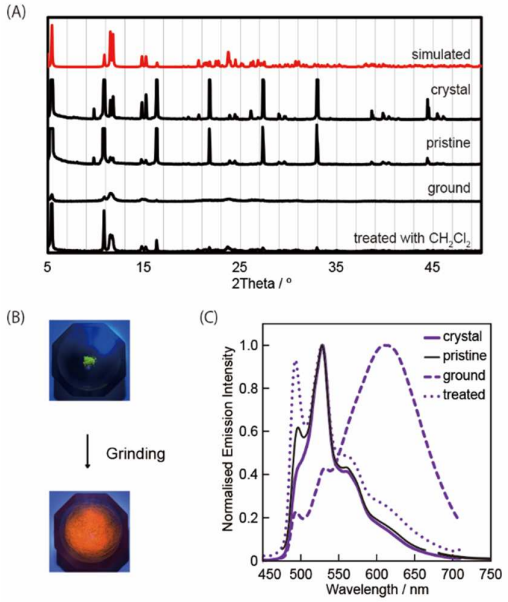

Fig. 5 (A) Changes in XRD patterns by mechanical grinding and solvent treatment for **1**. (B) Emission colour changes of **1** by grinding. (C) Luminescence spectral changes of **1** upon mechanical grinding and treatment with CH_2Cl_2 (λ_{ex} = 450 nm).

Pristine and crystal samples of **1** exhibited luminescent mechanochromic behavior in response to external stimuli (Fig. 5 and Table 2). When the both samples were ground or scratched, their green emission turned dramatically orange-red (Fig. 5B). Mechanical grinding resulted in decrease and increase in the peak intensities of the emission bands at 528 and 616 nm, respectively, (Fig. 5C), namely the emission maximum red-shifted by *ca.* 80 nm. Grinding gave little effect both on the quantum yield (Φ_{PL}) and on emission lifetime (τ_{em}) at room temperature: the pristine sample, Φ_{PL} = 0.14, τ_{em} = 0.81 μs; the ground sample, Φ_{PL} = 0.18, τ_{em} = 0.73 μs. (Table 2). Upon treatment of the ground sample with various solvents, the emission spectrum reverted to that of original pristine sample (Fig. 5C). Repeating of this cycle disclosed that the mechanochromic change in luminescence is reversible. Mechanical force led to change in emission colour as noted above, but not in absorption colour. The ground sample remained yellow colour, and the UV-Vis absorption spectrum displayed no significant shift, but a slight broadening of the lowest energy band further to lower energy side. Therefore, mechanical force does not significantly affect the energy gap between the ground state and the singlet excited state, but does the relative energy level of the triplet state in the amorphous solid. The phenomenon is characteristic point of the complex, since luminescent mechanochromism of previously reported cyclometalated complexes were derived from changes in the magnitude of the intermolecular Pt–Pt interactions, *i.e.* transformation of the molecular arrangement accompanied by the changes in absorption colours.[6]

The pristine and crystal samples of **2** also showed almost the same luminescent mechanochromic behaviour as those of **1**. The emission maxima shifted from 536 nm in the original state to 605 nm upon grinding (Fig. S3A ESI†).

Structures and luminescent mechanochromism of [Pt^{II}(ppy)Leu] (3) in the solid state

The pristine sample was obtained by addition of hexane into the solution in CH_2Cl_2. Solvent vapour diffusion of hexane into a solution of the pristine sample in CH_2Cl_2 provided yellow crystals suitable for X-ray analysis. The crystallographic data are summarised in Table S2, ESI†. TGA of the crystal sample showed absence of solvent molecules in the crystal (Fig. S4, ESI†).

Four crystallographically different complexes from each other were present in one cell unit. All these complexes are similar neutral molecules to those of **1** and **2**. Adjacent two complexes form a dimeric unit in a face-to-face arrangement through Pt–Pt and π–π interactions (Fig. 6). Rest two molecules form another dimeric unit. The intra-dimer Pt–Pt distances, the interplanar distances, and bite angles between the two ppy planes were 3.14 Å, 3.55 Å, and 8.69°, and 3.38 Å, 3.60 Å, and 7.57°, respectively. The Pt–Pt distances inside the dimeric units are significantly shorter than twice the van der Waals radius of Pt, suggesting the presence of metallophilic interactions, but no Pt–Pt and π–π interactions between dimers.

A comparison of the dimeric structures of **3** with monomeric ones of **1** and **2** suggests that steric hindrance of R_2 influenced significantly on the dimerisation. Complexes **1** and **2** with less bulky substituents showed higher planarity of the molecules, and they stacked to form columns. On the other hand, **3** formed a discrete dimeric unit having a Pt–Pt interaction, face-to-face stacked arrangement of ppy moieties, and anti-configuration of bulky substituents to avoid steric hindrance. The steric effect of R_2 on crystal arrangement was supported by the relationship between bulkiness of R_2 and features of the luminescence for **4** and **5**, see below.

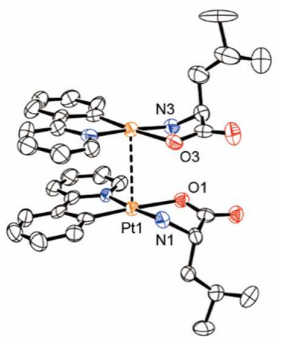

Fig. 6 Dimeric structure of **3** with thermal ellipsoids at the 50% probability level. Hydrogen atoms are omitted for clarity.

The similarity in XRD patterns of the pristine and crystal samples reveals that both samples have similar crystal structures to each other. Complex **3**, similarly with **1** and **2**, exhibited reversible conversion to amorphous phase by mechanical grinding, and to crystalline phase by treatment with solvent (Fig. 7C).

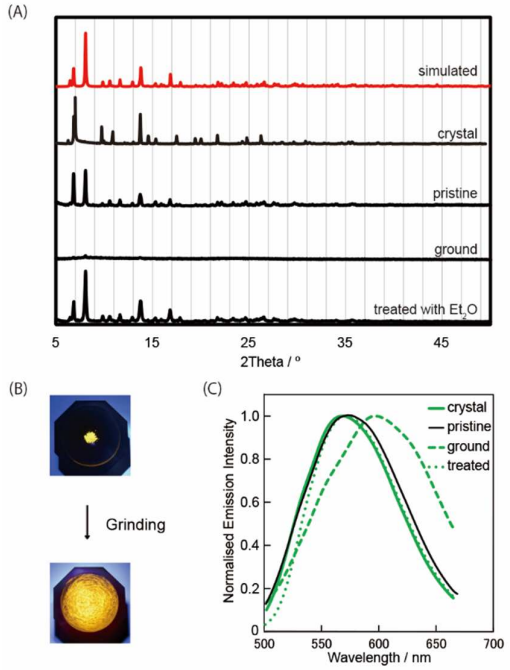

Fig. 7 (A) Changes in XRD patterns by mechanical grinding and solvent treatment for **3**. (B) Emission colour changes of **3** by grinding. (C) Luminescence spectral changes of **3** upon mechanical grinding and treatment with Et_2O (λ_{ex} = 450 nm).

The pristine and crystal samples showed yellow emission. The spectral patterns are similar to each other, and different from that in solution (Figs. 1 and 7, Tables 1 and 2). The crystal exhibited an emission maximum at 569 nm, red-shifted from *ca*. 510 nm in solution. The occurrence of the intra-dimer Pt–Pt interaction results in the splitting of degenerated d_z^2 orbitals to make a HOMO level higher and to let the emission red-shifted. The comparison of luminescence of **3** with those of **1** and **2** reveals that the colour of emission, *i.e.* total outlook of summation of the components and the intensity, the maximum wavelengths, band widths, etc., is significantly influenced by the molecular arrangement in the solid state, such as monomeric or dimeric structures, intermolecular interactions, etc.

The pristine and crystal samples of **3** also showed a reversible mechanochromism. Red-shift of the emission band to at 597 nm was observed on mechanical grinding, and treatment of the ground samples with CH_2Cl_2 restored the emission band perfectly to that of the original sample (Figs. 7B and 7C and Table 2). Grinding gave little effect both on the quantum yield (Φ_{PL}) and on emission lifetime (τ_{em}) at room temperature: the pristine sample, Φ_{PL} = 0.09, τ_{em} = 0.60 µs; the ground sample, Φ_{PL} = 0.04, τ_{em} = 0.55 µs. (Table 2). UV-vis absorption spectrum of the ground sample displayed no red-shift but slight increase in the intensity of the lowest-energy broad band from those of the pristine sample (Fig S5C, ESI†), indicating little change in molecular arrangements by grinding. The nature of the luminescence from the dimeric unit (^{3}MMLCT) remained essentially unchanged, but the relative energy level of the triplet state in amorphous state changed slightly by the application of the force.

Luminescent mechanochromism of [Pt^{II}(ppy)Ile] (4) in the solid state

The pristine polycrystalline solid was obtained by addition of hexane into the CH_2Cl_2 solution. Diffusion of hexane vapour into the solution of the pristine sample in CH_2Cl_2 provided yellow crystals, which exhibited yellow emission. TGA showed that none of these crystals contained solvent molecules (Fig. S4, ESI†).

The XRD analyses indicate reversible conversion between crystalline phase of original and solvent-treated samples and amorphous phase of the ground sample (Fig. S6). Both the crystal and pristine samples showed the different intense and sharp reflection patterns from each other, indicating difference in the molecular arrangements in crystalline state. Upon grinding of both samples, the reflections became weak and broadened showing the change into an amorphous phase. The treatment of the ground samples with CH_2Cl_2 restored the reflections to a similar pattern to that of the original crystal sample, *i.e.* no restoration of molecular arrangement to that of the original pristine sample. These results indicate that molecular arrangement of the crystal sample is more stable than that of the pristine sample.

The emission maxima of the crystal and pristine samples at 572 and 587 nm, respectively, exhibited red-shifts from that in solution and located in a similar region to that of crystal of **3** (Fig. 1 and Table 2). The results suggest Pt–Pt interaction in the solid state, and the difference of emission maxima may be derived from different magnitudes of the Pt–Pt interactions, since both samples exhibited different XRD patterns from each other.

The crystal sample showed reversible luminescent mechanochromic behaviour (Fig. S6, ESI† and Table 2). Mechanical grinding led to a red-shift of the emission band to at 592 nm, and treatment with CH_2Cl_2 restored the emission band to that of original crystal sample. Since the original

pristine sample showed the emission at 587 nm, the extent of the red-shift on the mechanical grinding is little (Fig. S6, ESI† and Table 2). Interestingly, treatment of the ground sample with CH_2Cl_2 resulted in a blue-shift of the emission band to that of crystal sample at ca. 575 nm. These result suggest that mechanical force and followed by treatment with solvent lead to luminescence changes from emission of the crystalline pristine sample to one of the crystal sample *via* emission of amorphous state of the ground sample. The UV-Vis absorption spectra of the ground sample displayed a slight broadening of the low-energy UV-vis absorption from that of the ground sample (Fig S5D, ESI†).

Luminescent mechanochromism of [Pt^{II}(ppy)Phe] (5) in the solid state

The pristine sample was obtained by addition of hexane into a solution in CH_2Cl_2. Recrystallisation from hot solution in EtOH provided yellow crystals with orange emission. TGA of these crystals showed the absence of lattice solvent molecules (Fig. S4, ESI†).

The XRD analyses indicate that amorphous state is more stable than crystalline state. The XRD pattern of the crystal sample showed sharp reflections, while the pristine, ground, and solvent-treated samples exhibited broad reflections. (Fig. 8A). The observations reveal that a changeover of molecular arrangements from a crystalline state of crystal sample to an amorphous state of the ground sample takes place, while there is no rearrangement of amorphous state to crystalline state by treatment of the ground sample with solvent. These results suggest that the amorphous state is kinetically and thermodynamically stable than crystalline one.

Luminescence of the crystal sample showed that the crystallisation caused a red-shift of the emission maximum to 591 from 525 nm in solution (Fig. 1 and Tables 1 and 2), and this shift is a similar situation to the crystallisations of **3** and **4** (see above). The pristine sample showed a broad emission band with emission maximum at 597 nm, and this wavelength is comparable to that of its crystal sample. These results suggest intermolecular Pt–Pt interaction in crystal and pristine samples.

Mechanochromism was not observed for **5**. Upon grinding, the crystals led to the broadening of emission band along with a very slight red-shift of the maximum by 6 nm (Fig. 8B and Table 2), while the pristine samples showed no shift and no broadening of emission band. Treatment of the ground samples with various general solvents, such as H_2O, EtOH, Et_2O, CH_2Cl_2, resulted in no change in the luminescence, *i.e.* the emission maximum and spectrum pattern remained unchanged. Recrystallisation of the ground sample, by vapour diffusion of hexane into the solution in CH_2Cl_2, induced restoration of emission band in similar region to that of the original crystal. These observations suggest, as well as the XRD results, that the pristine, ground, and solvent-treated samples are in an amorphous state, which is thermodynamically more stable than that of the crystal sample. The similarity of the UV-Vis absorption spectra of the pristine and ground samples supports the interpretation that there is no transformation of the molecular arrangement by grinding (Fig S5E, ESI†).

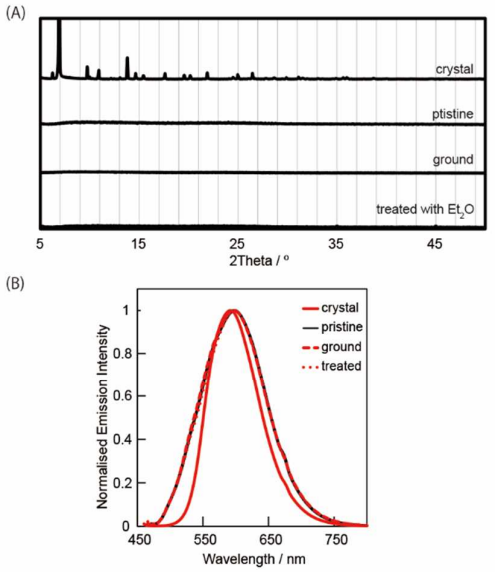

Fig. 8 (A) Changes in XRD patterns by mechanical grinding and solvent treatment for **5**. (B) Luminescence spectral changes of **5** upon mechanical grinding and treatment with Et_2O (λ_{ex} = 450 nm).

Polymorphs and luminescent mechanochromism of [Pt^{II}(ppy)Sar] (6) in the solid state

Addition of liquid hexane into the solution in CH_2Cl_2 gave yellow powder (pristine sample). Vapour diffusion of hexane into the solution of **6** in CH_2Cl_2 provided two kinds of crystals suitable for the X-ray analysis, *i.e.* yellow-green emitting (Crystal-G) and yellow emitting (Crystal-Y) ones, which were separated manually under a UV lamp (Fig. 9).

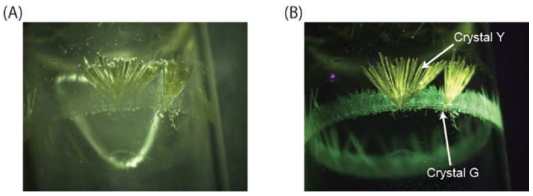

Fig. 9 Crystal-G and Crystal-Y under ambient light (A) and UV light with λ_{ex} = 365 nm (B).

The Crystal-G and Crystal-Y are crystalised in monoclinic *P*2(1)/*c* and in monoclinic *C*2/*c*, respectively. One unit-cell of Crystal-G contained two crystallographically different complexes and one lattice solvent, 2[Pt^{II}(ppy)Sar]·CH_2Cl_2, and that of Crystal-Y consisted of one complex and one lattice solvent, [Pt^{II}(ppy)Sar]·CH_2Cl_2, indicating that these crystals are pseudo-polymorphs. These crystallographic data are summarised in Table S2, ESI†.

The complexes in both crystals were neutral molecule with a similar structure to each other. Prochiral Sar$^-$ gave chiral complexes on coordination to the Pt^{II} centre, which is in square-planar geometry with trans-*N,N* configurations, as shown in Fig. 10. The methyl group on Sar$^-$ occupies an axial

position to the {PtN_2CO} coordination plane. In both the crystals enantiomeric pairs of the complex are packed in racemic arrangements with a chiral centre on N atom.

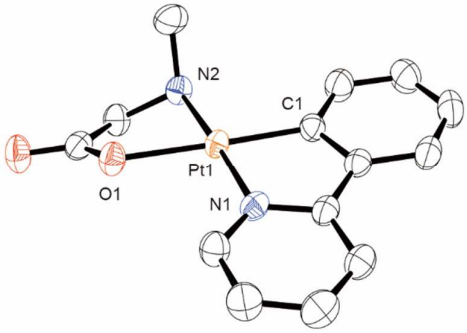

Fig. 10 Molecular structure of [Pt^{II}(ppy)Sar] in Crystal-G with thermal ellipsoids at the 50% probability level. The H atoms have been omitted for clarity.

In Crystal-G, the complexes are present both in a monomeric form (Pt1) and dimeric structures consist of two mononuclear complexes (Pt2 and Pt2A) through π-stacking, as shown in Fig 11A. These complexes are assembled in a three dimensional (3D) network through hydrogen bonds between Sar$^-$ moieties. The Pt1 complex bridges two adjacent dimeric units through two hydrogen bonds, (Pt2A)C=*O*···H–*N*(Pt1) and (Pt1)C=*O*···H–*N*(Pt2) (Table S3, ESI†). On the other hand, in dimeric units, the π–π interaction gives a head-to-tail configuration with the separation of 3.43 Å between ppy planes (Fig 12A).

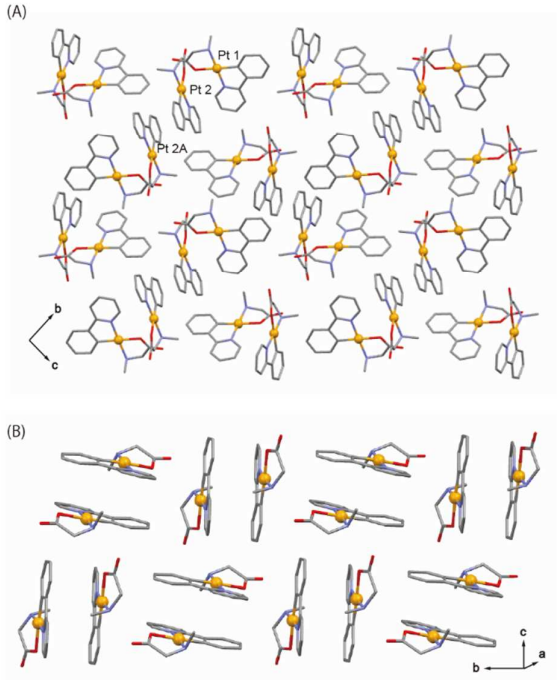

Fig. 11 (A) Crystal structure of Crystal-G. The Pt1 complex is in a monomer form, and the Pt2 and Pt2A complexes constitute a dimeric structure through π–π interaction. (B) Crystal structure of Crystal-Y. The complexes form dimeric structure with adjacent complex through π–π interaction.

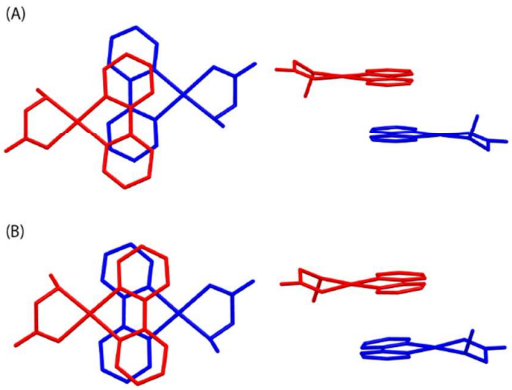

Fig. 12 The π–π stacking between ppy moieties in Crystal-G (A) and Crystal-Y (B).

In Crystal-Y, the adjacent two complexes formed a π-stacked dimeric structure with a head-to-tail configuration, and the dimer units were assembled in a two dimensional (2D) sheets through hydrogen bonding (Figs. 11B and 12B). The chiral complex interacted with its enantiomer through π–π interactions with the ppy separation of 3.46 Å, resulting in a racemic arrangement. The dimers were arranged perpendicularly to adjacent units through hydrogen bonds at C=*O*···H–*N* (Table S3, ESI†). These π–π interactions and hydrogen bonds led to the formation of the 2D sheet arrangement in crystal.

Comparison of the crystal structures of **6** to that of **3** suggest that the substituent R_1 influenced on conformations of stacked structures. Complexes form a face-to-face (anti-) π–π stacked dimer arrayed in a head-to-tail fashion, while **3** adopts a head-to-head arrangement. The difference originates from the steric effect of R_1, and the methyl group on the nitrogen of **6** prevents the head-to-head arrangement.

The XRD analyses of the pristine, Crystal-G, and Crystal-Y exhibited different molecular arrangements from each other, and the pristine sample is more stable crystalline state than others. All those samples showed intense and sharp reflections in their XRD patterns. Grinding these samples resulted in the conversion to an amorphous phase, since the ground samples exhibited no significant reflections and the patterns correspond to those seen for amorphous states. Treatment of the ground samples with CH_2Cl_2 restored the pattern to that of the pristine sample. These phase transformations are not caused by adsorption and desorption of lattice solvate molecules, because no signals of CH_2Cl_2 in the pristine and in solvent-treated samples were observed by ^{1}H NMR in DMSO. These observations exhibit that molecular arrangements of the pristine sample are thermodynamically more stable than those of crystal samples.

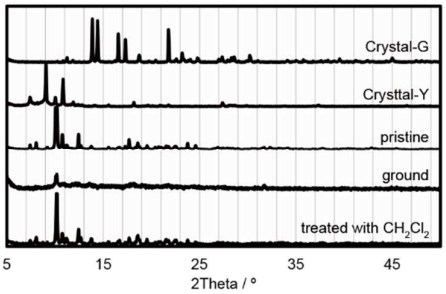

Fig. 13 The XRD analyses of the pristine, ground, and solvent-treated samples, Crystal-G, and Crystal-Y of [Pt^{II}(ppy)Sar].

The luminescence spectra in the solid state reveal that the luminescence of pristine sample, Crystal-G, and Crystal-Y originate from monomer, monomer, and both dimer and monomer, respectively, as shown in Fig. 14. The pristine sample and Crystal-G with green emission exhibited similar spectral pattern to each other and to that in solution, although the XRD reflections of both samples showed different patterns from each other (Fig. 13). The results suggest that both Crystal-G and pristine sample contain monomeric complexes, and dimeric units in Crystal-G show little effect on luminescence. Crystal-Y exhibited a broad emission band in the range of 490–660 nm with a maximum at 533 nm. The characteristic pattern is derived from the significant intra-dimer π–π interactions, because the crystal consists of only dimeric units. These results indicate that difference in the emission of Crystal-G from that of Crystal-Y comes from the presence of the monomeric structure.

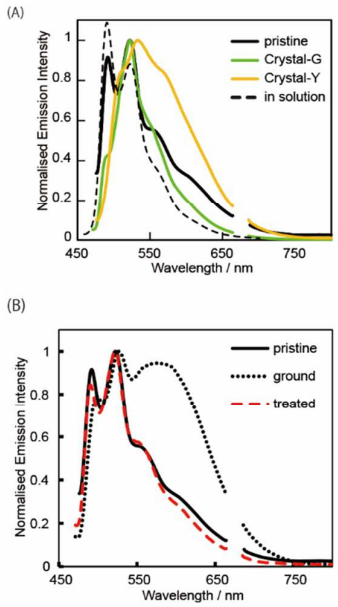

Fig. 14 (A) Normalised luminescent spectra (λ_{ex} = 450 nm) of Crystal-G, and Crystal-Y, and pristine sample of [Pt^{II}(ppy)Sar]. (B) Luminescence spectral changes upon mechanical grinding and treating with CH_2Cl_2 (λ_{ex} = 450 nm).

The pristine sample (green emission) exhibited luminescent mechanochromism (Figure 14B), and the resulted ground sample showed yellow emission. Upon grinding of the pristine sample, the sharp and intense emission band at 522 nm broadened and red-shifted slightly to 526 nm, and the broad emission band at 578 nm appeared. In addition, a sharp band at 492 nm decreased in the peak intensity along with a slight red-shift by 6 nm. When the ground sample was treated with CH_2Cl_2, emission bands were restored perfectly to those of the pristine sample. During these processes almost no change in the colour and the UV-Vis absorption maxima were observed except the slight broadening to the low-energy side of the band (Fig S5F, ESI†), indicating that the pristine and ground samples have similar magnitudes of the intermolecular interactions with each other. These results reveal that luminescence of the ground sample is a mixture of emissions from modified triplet state inside the dimer and from the original monomeric complex.

Crystal-G showed non-mechanochromism. The grinding followed by the treatment with CH_2Cl_2 did not restore the sample to Crystal-G, but gave the species very similar to the pristine sample, as suggested from the results of the XRD measurements, although the emission is almost the same (Fig 14). The ground sample showed entirely the same luminescent features as that of the pristine.

Conclusion

Luminescence properties of six newly synthesised cyclometalated platinum(II) complexes with α-aminocarboxylato (L), [Pt^{II}(ppy)L] (LH = Gly; Ala; Leu; Ile; Phe; Sar), in solution and in the solid state were discussed. The complexes exhibited interesting reversible luminescent mechanochromism in response to mechanical grinding and treatment with solvent for [Pt^{II}(ppy)L] (LH = Gly; Ala; Leu; Ile; Sar). The mechanochromism are derived from the change in the energy level of the triplet state due to the change in the extent of intermolecular interactions appeared as the crystalline–amorphous phase conversion, but not from variation in the nature of the luminescence, *i.e.* ^{3}MLCT for monomers, ^{3}MMLCT for dimers. The two pseudo-polymorphs of [Pt^{II}(ppy)Sar] showed different emission colours with each other, originating from the difference in the magnitude of intermolecular π–π interactions.

Experimental

General Procedures

All reagents were purchased from commercial sources and used without further purification. The platinum(II) dichloro-bridged dimer, [{Pt^{II}(ppy)}$_2$(μ-Cl)$_2$], were synthesized according literature.[9] Target complexes, [Pt^{II}(ppy)L] (LH = Gly (**1**), Ala (**2**), Leu (**3**), Ile (**4**), Phe (**5**), Sar (**6**)), were prepared by a modification of the literature method.[10]

The ^{1}H and ^{13}C NMR spectra were recorded on spectrometers Bruker AVANCE–400 with an internal reference $(CH_3)_4Si$ (δ = 0) in DMSO-d_6. The UV-vis and emission spectra were recorded

on a JASCO V-530, V-550 and FP-6600 spectrometer, respectively. The luminescence quantum efficiency was recorded on a HAMAMATSU C9920-02 absolute photoluminescence quantum yield measurement system equipped with an integrating sphere apparatus and 150 W CW xenon light source. The luminescence lifetime of each sample was recorded using a HAMAMATSU C11367-04 fluorescence lifetime measurement system using an LED laser at 405 nm excitation. The elemental analyses were carried out using FISONS EA 1112 and FISONS EA 1108 at the Comprehensive Analysis Center for Science, Saitama University. The powder X-ray diffraction (XRD) were obtained by using a Bruker AXS D2 PHASER. The thermogravimetric analyses (TGA) were performed with SII EXSTAR TG/DTA 6200. Single crystal X-ray data were collected using MoKα (λ = 0.71073 Å) radiation on a BRUKER APEX II Ultra diffractometer equipped with a CCD area detector. Indexing was performed using APEX2.[11] Data integration and reduction were performed using SaintPlus 6.01.[12] Absorption corrections were performed by a multiscan method implemented in SADABS.[13] Space groups were determined using XPREP implemented in APEX2. All structures were solved using direct method and refined using the SHELXL-97 (full-matrix least-squares on F^2) in the APEX2.[14] All non-hydrogen atoms for all complexes were refined anisotropically. Hydrogen atoms expect N–*H* of Crystal-G and Crystal-Y were refined using a riding model for all the complexes.

Computational Studies

Quantum mechanical calculations were performed using the *Gaussian 09W* program suit.[15]Geometry optimization for the ground state was carried out using the density functional theory (DFT) method with the B3LYP[16] hybrid exchange correlation functional implemented in the Gaussian suite of program and were followed by frequency calculations in order to verify that the obtained stationary points were true energy minima. The 6-31G* basis set[17] was used for all atoms except for the Pt atom, which was treated with LANL2DZ effective core potentials (ECPs) and corresponding basis sets.[18] Time-dependent density functional theory (TD-DFT) calculations were carried out with the same functional and basis sets as DFT calculation. All calculations were performed in DMSO using the polarizable continuum model (PCM) for the solvent.[19]

Procedure for the observation of mechanochromism

Mechanical stimuli to the pristine and crystal samples were inflicted by grinding with an agate mortar or scratching on paper with a spatula. Treatment of the ground samples was performed by a few drops of solvent.

Syntheses

[Pt^{II}(ppy)(Gly)] (Gly$^-$ = glycinate; 1)

The platinum(II) dichlorido-bridged dimer [{Pt^{II}(ppy)}$_2$(μ-Cl)$_2$] (0.12 g, 0.15 mmol), glycine (0.042 g, 0.56 mmol), and 28% sodium methylate methanol solution (0.072 g, 0.37 mmol) in methanol (30 mL) was refluxed for 18 h. After cooling to room temperature, the suspension was filtered off to obtain yellow-green powder, which was then washed with water and diethyl ether, and dried in vacuo. Yield: 80%. ^{1}H NMR (400 MHz, DMSO-d_6): δ 3.38 (t, 2H), 6.03 (t, 2H), 7.05 (m, 2H), 7.14 (m, 1H), 7.37 (m, 1H), 7.63 (d, 1H), 7.99 (d, 1H), 8.07 (t, 1H), 8.72 (d, 1H). ^{13}C NMR (400 MHz, DMSO-d_6): δ 46.87, 118.95, 122.61, 122.89, 123.73, 129.11, 132.75, 138.61, 139.43, 144.58, 148.70, 165.61, 180.43. UV-vis (DMSO) at room temperature, λ_{max} nm (ε/M^{-1}cm^{-1}): 316 (sh, 8500), 344 (sh, 4300), 380 (2800). Anal. calcd for $C_{13}H_{12}N_2O_2Pt$: C, 36.88; H, 2.86; N, 6.62. Found: C, 36.87; H, 2.80; N, 6.37.

[Pt^{II}(ppy)(Ala)] (Ala$^-$ = alaninate; 2)

The platinum(II) dichlorido-bridged dimer [{Pt^{II}(ppy)}$_2$(μ-Cl)$_2$] (0.083 g, 0.11 mmol), l-alanine (0.031 g, 0.35 mmol), and 28% sodium methylate methanol solution (0.049 g, 0.25 mmol) in methanol (30 mL) was refluxed for 18 h. After cooling to room temperature, the solvent was removed under reduced pressure. The residue was dissolved in dichloromethane and methanol, and insoluble salt was centrifuged off. The solution was concentrated, and diethyl ether was added to precipitate a yellow powder. The resulting yellow powder was filtrated out, and dried in vacuo. Yield: 92%. ^{1}H NMR (400 MHz, DMSO-d_6): δ 1.33 (d, 3H), 3.46 (m, 1H), 5.67 (dd, 1H), 6.26 (dd, 1H), 7.04 (m, 2H), 7.26 (d, 1H), 7.36 (t, 1H), 7.63 (d, 1H), 7.98 (d, 1H), 8.07 (t, 1H), 8.72 (d, 1H). ^{13}C NMR (400 MHz, DMSO-d_6): δ 19.58, 54.00, 118.91, 122.54, 122.81, 123.70, 129.05, 133.30, 139.10, 139.39, 144.64, 148.47, 165.68, 181.70. UV-vis (DMSO) at room temperature, λ_{max} nm (ε/M^{-1}cm^{-1}): 318 (sh, 7900), 347 (sh, 4200), 391 (2800). Anal. calcd for $C_{14}H_{14}N_2O_2Pt$: C, 38.45; H, 3.23; N, 6.41. Found: C, 38.40; H, 3.17; N, 6.29.

[Pt^{II}(ppy)(Leu)] (Leu$^-$ = leucinate; 3)

The platinum(II) dichlorido-bridged dimer [{Pt^{II}(ppy)}$_2$(μ-Cl)$_2$] (0.079 g, 0.10 mmol), l-leucine (0.030 g, 0.23 mmol), and 28% sodium methylate methanol solution (0.041 g, 0.21 mmol) in methanol (30 mL) was refluxed for 18 h. After cooling to room temperature, the solvent was removed under reduced pressure. The residue was dissolved in dichloromethane, and insoluble salt was centrifuged off. The solution was concentrated, and *n*-hexane was added to precipitate a yellow powder. The resulting yellow powder was filtrated out, and dried in vacuo. Yield: 93%. ^{1}H NMR (400 MHz, DMSO-d_6): δ 0.90 (d, 3H), 0.92 (d, 3H), 1.58 (m, 1H), 1.70 (m, 1H), 1.92 (m, 1H), 3.37 (m, 1H), 5.50 (dd, 1H), 6.30 (dd, 1H), 7.04 (m, 2H), 7.29 (d, 1H), 7.36 (t, 1H), 7.63 (d, 1H), 7.98 (d, 1H), 8.07 (t, 1H), 8.73 (d, 1H). ^{13}C NMR (400 MHz, DMSO-d_6): δ 21.74, 22.86, 23.53, 42.95, 56.25, 118.90, 122.51, 122.79, 123.63, 128.95, 133.48, 139.28, 139.37, 144.61, 148.51, 165.72, 181.75. UV-vis (DMSO) at room temperature, λ_{max} nm (ε/M^{-1}cm^{-1}): 317 (sh, 6500), 345 (sh, 3400), 392 (2200). Anal. calcd for $C_{17}H_{20}N_2O_2Pt$: C, 42.59; H, 4.21; N, 5.84. Found: C, 42.48; H, 4.19; N, 5.60.

[Pt^{II}(ppy)(Ile)] (Ile$^-$ = isoleucinate; 4)

The synthetic procedure for **4** was the same as that for **3** except using l-isoleucine.

Yield: 90%. ^{1}H NMR (400 MHz, DMSO-d_6): δ 0.88 (t, 3H), 1.05 (d, 3H), 1.40 (m, 1H), 1.52 (m, 1H), 1.90 (m, 1H), 3.37 (m, 1H), 5.14 (dd, 1H), 6.33 (dd, 1H), 7.04 (m, 2H), 7.32 (d, 1H), 7.35 (t,

1H), 7.63 (d, 1H), 7.98 (d, 1H), 8.06 (t, 1H), 8.73 (d, 1H). ^{13}C NMR (400 MHz, DMSO-d_6): δ 11.94, 15.22, 24.29, 38.20, 61.96, 118.88, 122.48, 122.76, 123.58, 128.90, 133.66, 139.34, 139.39, 144.57, 148.56, 165.76, 180.59. UV-vis (DMSO) at room temperature, λ_{max} nm (ε/M^{-1}cm^{-1}): 316 (sh, 8100), 345 (sh, 3700), 391 (2600). Anal. calcd for $C_{17}H_{20}N_2O_2Pt$: C, 42.59; H, 4.21; N, 5.84. Found: C, 42.35; H, 4.11; N, 5.68.

[Pt^{II}(ppy)(Phe)] (Phe$^-$ = phenylalaninate; 5)

The synthetic procedure for **5** was the same as that for **3** except using l-phenylalanine.

Yield: 78%. ^{1}H NMR (400 MHz, DMSO-d_6): δ 2.99 (dd, 1H), 3.22 (dd, 1H), 3.64 (m, 1H), 5.43 (dd, 1H), 6.32 (dd, 1H), 7.02 (m, 2H), 7.14 (d, 1H), 7.21 (t, 1H), 7.29 (t, 2H), 7.36 (m, 3H), 7.62 (d, 1H), 7.98 (d, 1H), 8.06 (t, 1H), 8.72 (d, 1H). ^{13}C NMR (400 MHz, DMSO-d_6): δ 59.35, 118.91, 122.54, 122.81, 123.64, 125.30, 126.16, 127.72, 128.15, 128.98, 129.25, 133.16, 137.99, 138.99, 139.42, 144.57, 148.51, 165.68, 180.57. UV-vis (DMSO) at room temperature, λ_{max} nm (ε/M^{-1}cm^{-1}): 316 (sh, 6500), 344 (sh, 3400), 391 (2200). Anal. calcd for $C_{20}H_{18}N_2O_2Pt$: C, 46.79; H, 3.53; N, 5.46. Found: C, 46.42; H, 3.46; N, 5.22.

[Pt^{II}(ppy)(Sar)] (Sar$^-$ = Sarcocinate; 6)

The platinum(II) dichloro-bridged dimer [{Pt^{II}(ppy)}$_2$(μ-Cl)$_2$] (0.080 g, 0.10 mmol), sarcosine (0.020 g, 0.22 mmol), and 28% sodium methoxide methanol solution (0.043 g, 0.37 mmol) in methanol (30 mL) was refluxed for 18 h. After cooling to room temperature, residual inorganic salts were removed by filtering. The target complex was obtained as a yellow solid by adding of hexane into a concentrated solution. Yield: 0.074 g (81%).

^{1}H NMR (400 MHz, DMSO-d_6): δ 2.79 (d, 3H), 3.23 (d, 1H), 3.80 (dd, 1H), 6.68 (dd, 1H), 7.08 (m, 2H), 7.28 (d, 1H), 7.36 (t, 1H), 7.65 (d, 1H), 7.99 (d, 1H), 8.06 (t, 1H), 8.68 (d, 1H). ^{13}C NMR (400 MHz, DMSO-d_6): δ 43.48, 58.17, 119.01, 122.82, 122.89, 123.80, 129.47, 132.43, 138.51, 139.74, 144.74, 148.72, 165.68, 178.37. UV-vis (DMSO) at room temperature, λ_{max} nm (ε/M^{-1}cm^{-1}): 318 (sh, 6000), 341 (sh, 3200), 388 (2100). Anal. Calcd for $C_{14}H_{14}N_2O_2Pt_1{\cdot}0.25CH_2Cl_2$: C, 37.32; H, 3.19; N, 6.11. Found: C, 37.04; H, 2.84; N, 5.87.

Acknowledgements

This work was supported by Grant-in-Aid for Scientific Research(C) (23510115 to T.F.) from the Japan Society for the Promotion of Science (JSPS). The authors express their heartfelt thanks to Profs. Takuji Hirose and Koichi Kodama and Dr. Hiroaki Shitara (Department of Applied Chemistry, Saitama University) for measurement of UV-Vis absorption spectra in the solid state. We thank Prof. Masa-aki Haga (Department of Applied Chemistry, Faculty of Science and Engineering, Chuo University) and Dr. Tomoaki Sugaya (Department of Chemistry and Biochemistry, School of Advanced Science and Engineering, Waseda University) for measurement and discussions for emission lifetimes. We thank Enago (www.enago.jp) for the English language review.

Notes and references

[a] Department of Chemistry, Graduate School of Science and Engineering, Saitama University, 255 Shimo-Okubo, Sakura-ku, Saitama 338-8570, Japan.
[b] Comprehensive Analysis Center for Science, Saitama University, 255 Shimo-Okubo, Sakura-ku, Saitama 338-8570, Japan.

† Electronic supplementary information (ESI) available. CCDC 1058377, (**1**); 1058376, (**2**); 1058378, (**3**); 1436036, (Crystal-G); 1436035, (Crystal-Y). For crystallographic data in CIF or other electronic format see DOI: 10.1039/b000000x/

1 (*a*) M. S. Lowry and S. Bernhard, *Chem. Eur. J.*, 2006, **12**, 7970; (*b*) Y. Chi and P.-T. Chou, *Chem. Soc. Rev.*, 2010, **39**, 638; (*c*) Q. Zhao, F. Li and C. Huang, *Chem. Soc. Rev.*, 2010, **39**, 3007; (*d*) G. Zhou, W.-Y. Wong and X. Yang, *Chem. Asian. J.*, 2011, **6**, 1706.
2 J. Brooks, Y. Babayan, S. Lamansky, P. I. Djurovich, I. Tsyba, R. Bau and M. E. Thompson, *Inorg. Chem.*, 2002, **41**, 3055.
3 (*a*) Á. Díez, J. Forniés, C. Larraz, E. Lalinde, J. A. López, A. Martín, M. T. Moreno and V. Sicilia, *Inorg. Chem.*, 2010, **49**, 3239; (*b*) R. Aoki, A. Kobayashi, H.-C. Chang and M. Kato, *Bull. Chem. Soc. Jpn.*, 2011, **84**, 218; (*c*) M. Ebina, A. Kobayashi, T. Ogawa, M. Yoshida and M. Kato, *Inorg. Chem.*, 2015, **54**, 8878.
4 (*a*) H. Yersin and G. Gliemann, Solid State. Comm. 1977, **21**, 915; (*b*) M. Kato, *Bull. Chem. Soc. Jpn.*, 2007, **80**, 218. (c) K. M.-C. Wong and V. W.-W. Yam, *Acc. Chem. Res.*, 2011, **44**, 424; (*d*) Y. Nishiuchi, A. Takayama, T. Suzuki and K. Shinozaki,*Eur. J. Inorg. Chem.*, 2011, 1815. (*e*) J. Forniés, V. Sicilia, P. Borja, J. M. Casas, A. Díez, E. Lalinde, C. Larraz, A. Martín and M. T. Moreno, *Chem. Asian J.* 2012, **7**, 2813.
5 (*a*) R. Valiente, J. M. García-Lastra, P. García-Fernández, S. García-Revilla and O. S. Wenger, *Eur. J. Inorg. Chem.*, 2007, 5735; (*b*) C. H. Shin, J. O. Huh, S. J. Baek, S. K. Kim, M. H. Lee and Y. Do, *Eur. J. Inorg. Chem.*, 2010, 3642; (c) S. Karasawa, R. Hagihara, Y. Abe, N. Harada, J. Todo and N. Koga, *Cryst. Growth Des.*, 2014, **14**, 2468.
6 (*a*) J. Ni, X. Zhang, N. Qiu, Y.-H. Wu, L.-Y. Zhang, J. Zhang and Z.-N. Chen, *Inorg. Chem.*, 2011, **50**, 9090; (*b*) J. Ni, X. Zhang, Y.-H. Wu, L.-Y. Zhang and Z.-N. Chen, *Chem. Eur. J.*, 2011, **17**, 1171; (*c*) X. Zhang, Z. Chi, Y. Zhang, S. Liu and J. Xu, *J. Mater. Chem. C*, 2013, **1**, 3376; (*d*) O. S. Wenger, *Chem. Rev.*, 2013, **113**, 3686; (e) A. Kobayashi and M. Kato, *Eur. J. Inorg. Chem.*, 2014, 4469; (*f*) J. Ni, Y.-G. Wang, H.-H. Wang, Y.-Z. Pan, L. Xu, Y.-Q. Zhao, X.-Y. Liu and J.-J. Zhang, *Eur. J. Inorg. Chem.* 2014, 986.
7 (*a*) T. Abe, T. Itakura, N. Ikeda and K. Shinozaki, *Dalton Trans.*, 2009, 711; (*b*) J. R. Kumpfer, S. D. Taylor, W. B. Connick and S. J. Rowan, *J. Mater. Chem.*, 2012, **22**, 14196; (*c*) X. Zhang, J.-Y. Wang, J. Ni, L.-Y. Zhang and Z.-N. Chen, *Inorg. Chem.*, 2012, **51**, 5569; (*d*) M. Krikorian, S. Liu and T. M. Swager, *J. Am.Chem. Soc.*, 2014, **136**, 2952; (*e*) A. Han, P. Du, Z. Sun, H. Wu, H. Jia, R. Zhang, Z. Liang, R. Cao and R. Eisenberg, *Inorg. Chem.*, 2014, **53**, 3338; (*f*) J. Ni, Y.-G. Wang, H.-H. Wang, L. Xu, Y.-Q. Zhao, Y.-Z. Pan and J.-J. Zhang, *Dalton Trans.*, 2014, **43**, 352.
8 N.Komiya, N. Itami and T. Naota, *Chem. Eur. J.*, 2013, **19**, 9497.
9 (*a*) D. M. Jenkins, J. F. Senn Jr. and S. Bernhard, *Dalton. Trans.* 2012, **41**, 8077; (*b*) L. Pazderski, T. Pawlak, J. Sitkowski, L. Kozerskib and E. Szłyka, *Magn. Reson. Chem.* 2009, **47**, 932.
10 R. Urban, R. Krämer, S. Mihan, K. Polborn, B. Wagner and W. Beck, *J. Organomet. Chem.*, 1996, **517**, 191.
11 Bruker (APEX2); Bruker AXS Inc.: Madison, Wisconsin, USA, 2008.

12 Bruker SAINT, Data Reduction Software; Bruker AXS Inc., Madison, Wisconsin, USA, 2008.
13 G. M. Sheldrick, SADABS. Program for Empirical Absorption Correction; University of Göttingen, Germany, 2008.
14 G. M. Sheldrick, *Acta Cryst.* 2006, **A24**, 112.
15 M. J. Frisch, G. W. Trucks, H. B. Schlegel, G. E. Scuseria, M. A. Robb, J. R. Cheeseman, G. Scalmani, V. Barone, B. Mennucci, G. A. Petersson, H. Nakatsuji, M. Caricato, X. Li, H. P. Hratchian, A. F. Izmaylov, J. Bloino, G. Zheng, J. L. Sonnenberg, M. Hada, M. Ehara, K. Toyota, R. Fukuda, J. Hasegawa, M. Ishida, T. Nakajima, Y. Honda, O. Kitao, H. Nakai, T. Vreven, J. A. Montgomery Jr., J. E. Peralta, F. Ogliaro, M. Bearpark, J. J. Heyd, E. Brothers, K. N. Kudin, V. N. Staroverov, R. Kobayashi, J. Normand, K. Raghavachari, A. Rendell, J. C. Burant, S. S. Iyengar, J. Tomasi, M. Cossi, N. Rega, J. M. Millam, M. Klene, J. E. Knox, J. B. Cross, V. Bakken, C. Adamo, J. Jaramillo, R. Gomperts, R. E. Stratmann, O. Yazyev, A. J. Austin, R. Cammi, C. Pomelli, J. W. Ochterski, R. L. Martin, K. Morokuma, V. G. Zakrzewski, G. A. Voth, P. Salvador, J. J. Dannenberg, S. Dapprich, A. D. Daniels, O. Farkas, J. B. Foresman, J. V. Ortiz, J. Cioslowski and D. J. Fox, *Gaussian 09, Revision C. 01*, Gaussian, Inc., Wallingford CT, 2009.
16 (*a*) A. D. Becke, *Phys. Rev. A: At., Mol., Opt. Phys.*, 1988, **38**, 3098; (*b*) A. D. Becke, *J. Chem. Phys.*, 1993, **98**, 5648; (*c*) C. Lee, W.Yang and R. G. Parr, *Phys. Rev. B*, 1988, **37**, 785; (*d*) T. Yanai, D. Tew and N. Handy, *Chem. Phys. Lett.*, 2004, **393**, 51.
17 P. C. Hariharan and J. A. Pople, *Theor. Chim. Acta*, 1973, **28**, 213−222.
18 P. J. Hay and W. R. Wadt, *J. Chem. Phys.*, 1985, **82**, 270.
19 (a) B. Mennucci, J. Tomasi, R. Cammi, J. R. Cheeseman, M. J. Frisch, F. J.; Devlin, S. Gabriel and P. J. Stephens, *J. Phys. Chem. A*, 2002, **106**, 6102. (b) R. Cammi and J. Tomasi, *J. Comput. Chem.*, 1995, **16**, 1449. (c) A. Miertuš, E. Scrocco and J. Tomasi, *Chem. Phys.*, 1981, **55**, 117.

Cyclometalated platinum(II) complexes with α-aminocarboxylato ligands, [Pt^{II}(ppy)L] (ppy = 2-phenylpyridinato, LH = Gly, Ala, Leu, Ile, Phe, Sar) in the solid state exhibited reversible luminescent mechano chromisms.